Dalton Transactions

Accepted Manuscript

ROYAL SOCIETY OF CHEMISTRY

www.rsc.org/dalton

Cite this: DOI: 10.1039/c0xx00000x

www.rsc.org/xxxxxx

ARTICLE TYPE

Reaction-based Turn-on Fluorescent Probes with Magnetic Responses for Fe^{2+} Detection in Live Cells

Siddhartha Maiti,[a,b,c] Ziya Aydin,[c,d] Yi Zhang,[a,c] and Maolin Guo,[a,b,c,d*]

Received (in XXX, XXX) Xth XXXXXXXXX 20XX, Accepted Xth XXXXXXXXX 20XX
DOI: 10.1039/b000000x

Iron is the most abundant nutritionally essential transition metal found in the human body. It plays important roles in various biological processes such as oxygen delivery, electron transport, enzymatic reactions and DNA synthesis and repair. However, iron can also catalyze the production of free radicals, which are linked to quite a few diseases such as cancer, neurodegenerative diseases, and cardiovascular diseases. Both iron deficiency and iron overload are related to various health problems. Thus, precisely monitoring iron ions (Fe^{2+} and Fe^{3+}) in biological systems is important in understanding the detailed biological functions of iron and its trafficking pathways. However, effective tools for monitoring labile Fe^{2+} in biological systems have not yet been established. Reported herein are turn on, reaction-based coumarin and rhodamine-linked nitroxide probes (Cou-T and Rh-T) for selective detection of Fe^{2+} in solution and in living cells. Rh-T displayed unique change in EPR signal as well as enhancement of fluorescence signal resulting from specific redox reaction between probe and Fe^{2+}. The turn-on fluorescence response towards Fe^{2+} allows the subcellular imaging of endogenous Fe^{2+} as well as under conditions of externally iron supplementation or depletion, with labile Fe^{2+}pool located in mitochondria of human fibroblast primary cells. The detection and mechanism were verified by the magnetic property of the probe via electron paramagnetic resonance (EPR) spectroscopy in solution and in cells.

INTRODUCTION

Iron is the most abundant nutritionally essential transition metal found in the human body [1, 2]. It is essential because it is the key part in the prosthetic group in heme containing proteins as well as non-heme iron containing proteins (such as Fe-S clusters) and thereby plays important roles in various biological processes such as oxygen delivery, electron transport, enzymatic reactions and DNA synthesis and repair [3]. However, cellular 'transit labile iron pools' are toxic to cells as the labile iron ions promote the production of reactive oxygen species(ROS) which is linked to the aging process and a few degenerative diseases [4,5]. In particular, ferrous iron (Fe^{2+}) when reacts with hydrogen peroxide, it produces hydroxyl radical, which is believed to be the most dangerous form of ROS in cells [6]. The 'transit' iron pool contributes to the cellular iron uptake via transferrin and it is believed that this 'transit' pool is in steady state equilibrium by binding tightly to iron metalloproteins or loosely attached to low molecular-weight compounds such as phosphate, carbonate and citrate [7, 8]. Disruption of iron equilibrium in cells is linked to a few diseases such as cancer, hepatitis and several neurological diseases including Alzheimer's disease and Parkinson's disease [9-11]. The labile iron pool where iron is loosely bound to small molecules is responsible for both iron toxicity and regulation of various cellular processes [12, 13]. However, the intracellular iron transport mechanisms, the biological functions of labile irons and their subcellular locations are still poorly understood because of lack of effective tools to monitor iron ions in living cells [14, 15].

Optical imaging with fluorescent sensors has gained much attention over the past few years in detecting metal ions such as zinc (II), copper (I), calcium (II) in living cells [16-18]. However, there are very few fluorescent sensors available for the detection of iron ions, especially iron (II), due to fluorescent quenching upon binding to iron ions as well as interference from other metal ions [19, 20]. For example, turn off sensors such as calcein and Phen Green SK are useful to detect intracellular "chelatable' iron but they suffer from interference from other metal ions [21, 22]. At present, a very few turn-on iron (II) sensors have been reported. For example, dihydrorhodamine 123 has shown indirect and non-selective turn on response to iron (II) as it detects reactive oxygen species (ROS) produced by iron (II)-catalyzed Fenton reaction [23-25]. Tang et al. reported a fluorescent probe for iron (II) detection in live HL-7702 and Hep G2 cells but the probe suffers from quenching effects of iron (II) through chelation[26]. DansSQ is another Fe^{2+}-selective sensor which consists of a danysl group-linked styrylquinoline which shows a 15-fold increase in fluorescence at 460 nm when it binds with

Fe^{2+} [27], however, this sensor suffers from interference from other metal ions as well as it is only soluble in organic solvents and thus is not suitable for bioimaging. Recently, reaction-based turn-on sensors, Rho-Nox1 [28] and IP1 [29] for Fe^{2+}-detection in cells have been reported, however, Rho-Nox1 located cellular Fe^{2+}signals in Golgi rather than mitochondria which is believed to be the major organelle store Fe^{2+} [30]; while IP1 displayed rather weak signal with poor spatial resolution, presumably due to the diffusive nature of the fluorophore liberated after reaction with Fe^{2+}.

Recently, we have been developing turn-on fluorescent sensors for imaging metal ions and oxidative stress in live cells [31-35]. Our turn-on Fe^{3+}sensor RPE has located the cellular Fe^{3+}-pools in mitochondria and endo/lysosomes for the first time. Here we describe the properties of highly selective and sensitive Fe^{2+} sensors Cou-T and Rh-T (Scheme 1) with unique Fe^{2+}-dependent fluorescent and magnetic properties. The turn-on fluorescence responses towards Fe^{2+} allows the subcellular imaging of endogenous Fe^{2+} as well as under conditions of externally iron supplementation or depletion, with labile Fe^{2+} pool located in mitochondria of human fibroblast primary cells for the first time. The detection and mechanism were verified by the magnetic property of the probe via electron paramagnetic resonance (EPR) spectroscopy in solution and in cells.

EXPERIMENTAL SECTION

Materials and instruments

Rhodamine B, coumarin-3-carboxylic acid, 4-hydroxy TEMPO, N, N-Dicyclohexylcarbodiimide (DCC), and 4-Dimethylaminopyridine (DMAP) were purchased from Sigma-Aldrich. The other chemicals and the solvents used in the experiments were purchased commercially. The solution of metal ions were prepared from chloride salts of Ni^{2+}, Fe^{3+}, Cu^{2+}, Mn^{2+}, Hg^{2+}, Na^{+}, Ca^{2+}, Zn^{2+}, Ag^{+}, and nitrate salts of Mg^{2+}, Pb^{2+}, K^{+}, Co^{2+}. Stock solutions of metal ions (10 mM) were prepared in deionized water, except for Cu^{2+} and Co^{2+}, which were dissolved in acetonitrile anhydrous. Solution of Cu^{+} was freshly prepared by dissolving tetrakis(acetonitrile)copper(I) (Sigma-Aldrich) into double-distilled water. Fe^{3+}, Fe^{2+} solutions were prepared freshly from ferric chloride, ferrous ammonium sulfate (FAS, $Fe(NH_4)_2(SO_4)_2$, respectively, in 0.1 M HCl.

A stock solution of **Cou-T** or **Rh-T** (1 mM) was prepared in DMF. The solution of **Cou-T** or **Rh-T** was diluted to 6 μM with MOPS buffer (10 mM, pH 7.3). In selectivity experiments, the test samples were prepared by appropriate amount of metal ion stock into 1 ml solution of **Cou-T** or **Rh-T** (6 μM). ESI-MS analyses were performed using a Perkin-Elmer API 150 EX mass spectrometer. UV/Vis spectra were recorded on a Perkin-Elmer Lambda 25 spectrometer at 293 K. Fluorescence spectra were recorded on a Perkin-Elmer LS55 luminescence spectrometer at 293 K. The pH measurements were carried out on a Corning pH meter equipped with a Sigma-Aldrich micro combination electrode calibrated with standard buffer solutions. EPR spectra were recorded on a Bruker e-scan spectrometer at room temperature.

Synthesis and Characterization

Coumarin-3-carboxylic acid or rhodamine B was esterified with 4-hydroxy-TEMPO in the presence of 1, 3-dicyclohexanecarbodiimide and 4-(dimethylamino) pyridine (DMAP) in CH_2Cl_2 under argon atmosphere for 2 h by a procedure similar to that described by Hassner [36].

More details: 4-Hydroxy TEMPO (0.2 g, 1.16 mmol), coumarin-3-carboxylic acid (0.10 g, 0.53 mmol), and DMAP (1.5 mg) were stirred in dry CH_2Cl_2 (5 mL) under nitrogen atmosphere. In a separate flask, DCC was diluted with dry CH_2Cl_2 (5 mL) and pyridine (0.1 g). This solution was then added by a syringe to the reaction mixture and stirred for 2 hours at room temperature under nitrogen atmosphere. The solvent was removed under reduced pressure to give the crude product, which was purified by silica gel flash chromatography using Hexane to Hexane/EtOAC (0 to 1;1) as eluent to afford the compound **Cou-T** (yield 72%). ESI-MS: found: m/z = 367.0 $[M+Na]^+$, 711.2 $[M+MNa]^+$ calcd for $C_{19}H_{22}NO_5Na^{+\cdot}$ = 367.38 (Figure S1).

Using a similar procedure with rhodamine B instead ofcoumarin-3-carboxylic acid, **Rh-T** was prepared (0.22 g, yield 67%). ESI-MS: found: m/z = 597.4 $[M]^+$ (without Cl^-), calcd for $C_{37}H_{47}N_3O_4^{+\cdot}$ = 597.7 (Figure S2).

Cell culture experiments and confocal fluorescence imaging experiments

Human primary fibroblast ws1 cells were grown at 37 ° C in a humid atmosphere of 5% CO_2 atmosphere in Eagle's minimum essential medium (EMEM, ATCC) supplemented with 10% fetal bovine serum (FBS, ATCC). Cultures were divided into 1:2 every 48 h to an approximate cell density of 1.21 million cells/ml and used for experiments after 24 h**.**

A Zeiss LSM 710 laser-scanning confocal microscope system was used for cell imaging experiments. 40x oil-immersion objective lens were used to perform all the experiments. For imaging with the **Rh-T** sensor, excitation wavelength of the laser was 543 nm and emissions were collected over the range 547-703 nm with image total acquisition time 1.54 sec for cells without tracker and 11.71 sec for cells with MitoTracker and Lyso Tracker. For images with MitoTracker Green FM, LysoTracker Blue DND-22, excitation wavelengths were set following the protocol provided by the manufacturer. Emissions were integrated at 492-548 nm (MitoTracker), 409-484 nm (LysoTracker), respectively.

Ws1 cells, at an approximately density of 1.2 million/ml in complete EMEM medium, were incubated with 100 μM ferrous ammonium sulfate (FAS, $Fe(NH_4)_2(SO_4)_2$ from a 10 mM stock solution) for overnight at 37 ° C in a humid atmosphere of 5% CO_2 and then the cells were washed with fresh EMEM medium to remove excess Fe^{2+}. Then cells were incubated with **Rh-T** (1 μM, from 500 μM stock solution in DMF) at 37 ° C for 30 min and then cells were washed with EMEM media and then imaged. In addition, some cells were treated firstly with 100 μM Fe^{2+} overnight and then the cells were washed with fresh EMEM medium. For chelation experiments, Fe^{2+}-loaded cells or untreated cells were incubated with 1 mM 2, 2'-bipyridyl (Bpy) at 37 °C for 30 min , then sensor was added followed by washing with the media, and then imaging was done. Controls were

imaged without incubation with Fe^{2+} or 2, 2'-bipyridyl.

EPR experiments:

EPR spectra were recorded on a Bruker e-scan spectrometer at room temperature. Instrument settings: microwave frequency, 9.75 GHz; microwave power, 12.17 mW; sweep width, 100 G; modulation amplitude, 3.06 G; time constant, 10.24 ms; conversion time, 5.12 ms; sweep time, 2.62 s. For EPR experiments with cells, the cells were treated with Fe^{2+}/Bpy/sensor exactly the same way as that was done for confocal experiments. After the incubation, cells were harvested by trypsinization and then were centrifuged. Aliquots of the concentrated cell pellets were immediately transferred to bottom-sealed Pasteur pipettes and the EPR spectra were recorded.

RESULTS AND DISCUSSION

Sensor design and Fe^{2+}-sensing mechanism

Inspired by an interesting fluorescence masking strategy via stable radical attachments [37], we covalently linked fluorophores with a Fe^{2+}-reacting nitroxide radical TEMPO. The tethering of a fluorophore to a nitroxide radical which first leads to a paramagnetic species with quenched (mask) fluorescence; upon reaction with Fe^{2+} in aqueous solution, the nitroxide radical could be converted to diamagnetic hydroxylamine with fluorescence recover (unmask)(Scheme 1). This strategy may be harnessed for Fe^{2+}sensing in biological systems.

The sensors **Cou-T** and **Rh-T**, combining a coumarin or a rhodamine reporter and a tempo receptor moiety for Fe^{2+} (Scheme S1), was synthesized by a one-step procedure (see supporting information, Scheme S1). The identity of the Cou-T and Rh-T radical was confirmed by ESI-MS and EPR (Figures S1-S3).

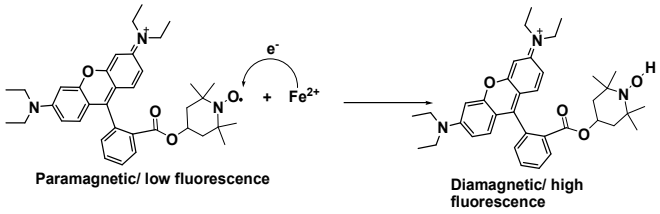

Scheme 1. The proposed sensing mechanism of reaction between **Rh-T** and Fe^{2+} in aqueous media.

Spectroscopic Properties

Cou-T and Rh-T both displayed the characteristic EPR splitting pattern of that of TEMPO (Fig. S3), confirming covalent links formed between the dyes and the TEMPO radical.

Rhodamine B displayed strong fluorescence emission in aqueous solution with an emission maximum at 580 nm. When it was linked to a stable nitroxide (TEMPO) radical moiety via ester bond, the original fluorescence intensity of rhodamine B was quenched (Figure S4) due to intra-molecular quenching (mask) [38]. Rh-T showed an absorption band (λ_{max} = 557 nm, ϵ = 41, 000 M^{-1} cm^{-1}) and weak fluorescence (Φ = 0.134, λ_{em}= 580 nm) (Figure 1A and Figure S4) in a physiological buffer (10 mM MOPs buffer, pH 7.3). We then evaluated the spectroscopic properties of **Rh-T** and its interactions with various metal ions. Addition of Fe^{2+} into Rh-T solution triggered a significant fluorescence enhancement (~2.5-fold), suggesting the reduction of the TEMPO species to the diamagnetic hydroxylamine [39-40] with fluorescence recovery (unmask). However, the fluorescence recovery did not fully reach to that of rhodamine B (Fig. S4), presumably due to the incomplete reaction and the presence of paramagnetic iron ions in the system. The reaction is reasonably fast and it takes ~ 25 min to reach the maximum fluorescence (Fig. S5). The fluorescence response to Fe^{2+} is semi-quantitative with a detection limit ~ 0.75 µM. However, 1 equiv was good enough to observe the intensity increase in fluorescence. **Cou-T** showed a similar fluorescence response towards Fe^{2+} but the fluorescence enhancement is weaker (~1.7-fold, data not shown). Subsequent experiments were thus more focused on **Rh-T.**

Excitingly, **Rh-T** displayed an excellent selective turn-on fluorescent response to Fe^{2+} (Figure 1B). In the presence of other bio-relevant metal ions including Fe^{3+}, Ni^{2+}, Cu^{+}, Cu^{2+}, Zn^{2+}, Pb^{2+}, Cr^{3+}, Hg^{2+}, Mn^{2+}, Ag^{+}, Co^{2+}, K^{+}, Na^{+}, Ca^{2+}, and Mg^{2+}; **Rh-T** did not trigger fluorescence enhancements under the same conditions (the grey bars in Figure 1B). Moreover, upon the addition of 1 equiv of Fe^{2+} into solutions containing one of the other metal ions tested, the fluorescence was activated and the intensity increased to a level similar to that observed in the presence of Fe^{2+} only (the black bars in Figure 1B). This demonstrated that these metal ions did not interfere with the response of Fe^{2+} to **Rh-T.**

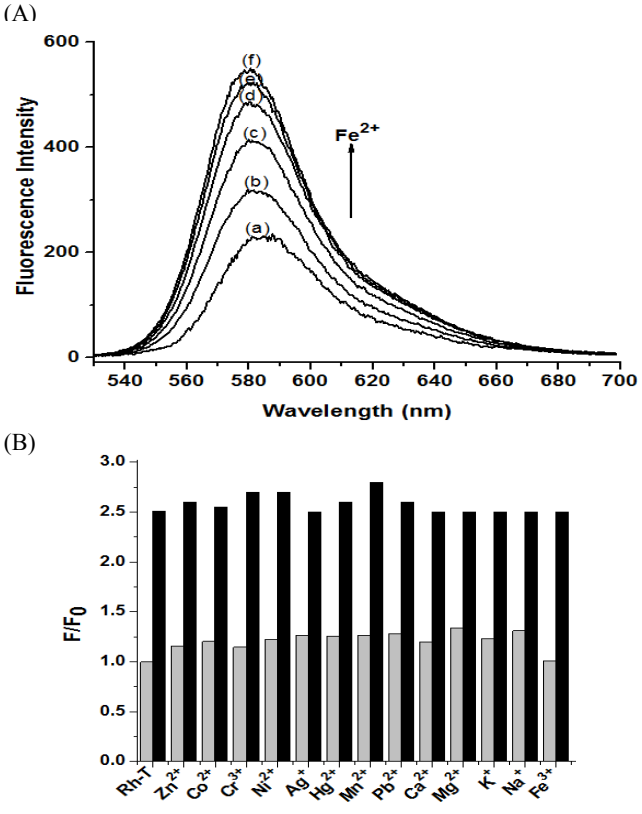

Fig.1. (A) Titration of 6 µM Rh-T (a) with 3 µM (b), 6 µM (c), 12 µM (d), 18 µM(e) and 24 µM (f) of Fe^{2+} in MOPs buffer (10 mM, pH 7.3). The intensities were collected 30 min after each addition. (B) Fluorescence responses of 6 µM Rh-T in the

presence of various metal ions (gray bar) and the subsequent addition of Fe^{2+} (black bar) in the MOPS buffer (10 mM, pH 7.3); the bars represent the fluorescence intensity at 580 nm.

We also monitored the interactions of **Rh-T** with Fe^{2+} and Fe^{3+} by EPR spectroscopy (Figure 2). The TEMPO-containing **Rh-T** molecule is paramagnetic in nature as it contains one unpaired electron. The EPR spectrum of **Rh-T** displays a typical TEMPO-type triplet (Figure 2a). The addition of 20 μM of Fe^{3+} to 6 μM Rh-T did not result in any change in the EPR spectrum of **Rh-T** which confirms no reaction of **Rh-T** with Fe^{3+} (Figure 2b). Whereas the triplet spectrum of **Rh-T** disappeared upon the addition of 20 μM of Fe^{2+} to **Rh-T** (Figure 2c), suggesting a reduction of the TEMPO moiety by Fe^{2+} which donates one electron to Rh-T and oxidized to Fe^{3+} (Scheme 1). Upon accepting the electron from Fe^{2+}, **Rh-T** becomes diamagnetic and hence the EPR signal disappears.

Because the oxidation ability of nitroxide moiety depends on the acidity of the system [41, 42], we investigated the effect of pH on the redox process and monitored by fluorescence spectroscopy. As seen in Figure S6, the fluorescence intensity of **Rh-T** itself is not affected by pH at the physiological pH range and so does the **Rh-T** + Fe^{2+} system which maintains a ~2.5-fold fluorescence enhancement compared to that of **Rh-T**. However, at pH below 6, the fluorescence intensity of **Rh-T** + Fe^{2+} system increased with the increase in acidity (increased ~ 40% by pH 5), consisting with that the redox process is more favored at acidic conditions [41-42].

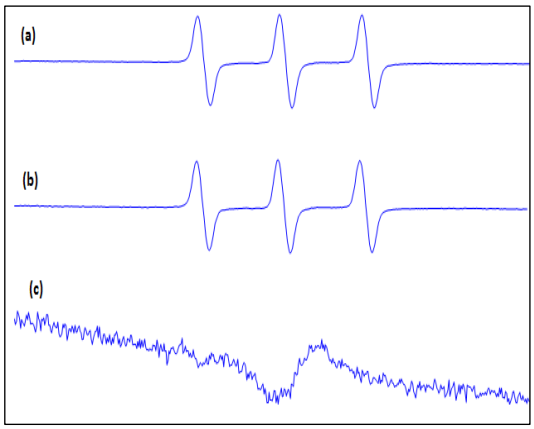

Fig. 2. EPR spectra of the sensor (6 μM) and its interactions with Fe^{2+} (20 μM) and Fe^{3+} (20 μM) in MOPs buffer (10 mM, pH 7.3) (a) Rh-T; (b) Rh-T + Fe^{3+}; (c) Rh-T+ Fe^{2+}.

The nitride oxide moiety could be sensitive for reacting with other biologically relevant free radical species [43], thus interfering with the desired Fe^{2+} detection in biological systems. We then investigated the reactivity of **Rh-T** with a few biologically relevant reactive radical species such as reactive oxygen species (ROS) and reactive nitrogen species (RNS) *in vitro* and monitored the reactions by fluorescence and EPR spectroscopies (Figures S7-S8 and Figure 3). Potassium superoxide (KO_2) was used to produce superoxide radicals ($O_2^{\cdot-}$) in solution; NOC-5 (1-Hydroxy-2-oxo-3-(3-aminopropyl)-3-isopropyl-1-triazene) which spontaneously generates nitric oxide radical ($NO^{\cdot}$) under physiological conditions [44] was used as $NO^{\cdot}$ source, SIN-1(3-(4-Morpholinyl) sydnonimine) was used to spontaneously generates peroxynitrite ($ONOO^-$) [45] while hydroxyl radicals ($HO^{\cdot}$) were generated in situ via Fenton reaction using Fe (II)-EDTA and H_2O_2 [46]. As seen in Figure 3, incubation of **Rh-T** with large excess of the ROS/RNS species H_2O_2, $O_2^{\cdot-}$, $NO^{\cdot}$ or $ONOO^-$ did not produce any changes in the EPR spectrum of **Rh-T** nor any enhancement in fluorescence (Fig. S8). Fe (II)-EDTA or H_2O_2 does not cause any enhancement in fluorescence of **Rh-T** (Fig. S7); only hydroxyl radical cause a slight enhancement in fluorescence (~30%, Fig. S7); however, this small enhancement is insignificant compared to that caused by Fe^{2+}. Considering that the concentrations of these ROS/RNS species in cells are much lower than those tested here, the ROS/RNS species is unlike to interfere with Fe^{2+}detection in cells.

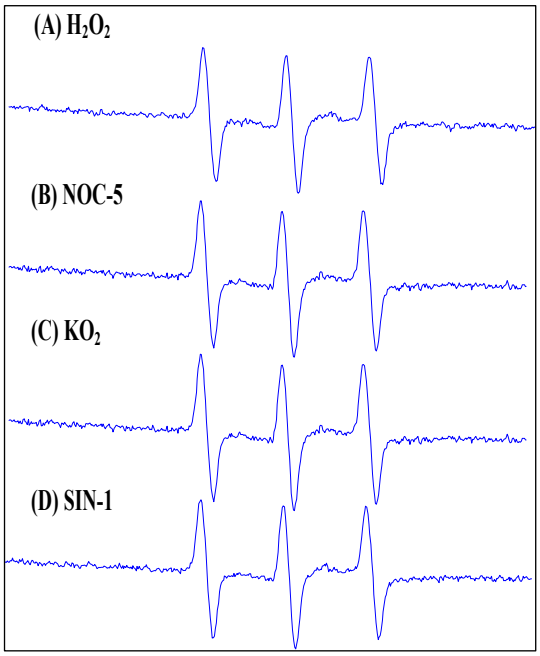

Fig. 3. EPR spectra of 6 μM Rh-T after incubation with ROS and RNS in KPB buffer (pH 7.4) (A) with 100 μM H_2O_2; (B) with 100 μM NOC-5; (C) with 50 μM NOC-5; (D) with 100 μM SIN-1.

Another possible source of interference is cellular reducing agents such as ascorbic acid, which has been shown to reduce nitroxide in unbuffered water solution [47]. This is also verified in our experiments (Figure S9) in which large excess (10 -fold) ascorbic acid caused ~150% fluorescence enhancement of **Rh-T** in unbuffered water solution (actual pH ~ 5.3). However, this reduction reaction is largely pH-dependent. Upon carrying out the reaction in more physiological pH (MOPS buffer, pH 7.3), the reaction is greatly diminished with fluorescence enhancement reduced to ~20% (Figure S10).

Nicotinamide adenine dinucleotide (NADH) which is found in cells is known to be a strong reducing agent. Cellular concentration of total NAD^+/NADH is ~ 365 ± 30.2 μM [48]. The reducing ability of nicotinamide adenine dinucleotide (NADH)

with the **Rh-T** probe was also tested for potential interference with Fe^{2+} detection. As shown in Figure S11, large excess of NADH (25-fold) does not cause any fluorescence enhancement of **Rh-T**, and at 365-fold excess (suppose all cellular NAD in its reduced form), only ~15% fluorescence enhancement was observed (Fig. S11). These data suggest that NADH does not significantly interfere with Fe^{2+} detection by **Rh-T** under cellular concentration. Based on the spectroscopic and interference studies, it is reasonable to hypothesize that under cellular conditions, Fe^{2+} is the major species responsible for **Rh-T** reduction and the associated fluorescence enhancement. Confocal imaging studies with live cells were then performed to test the ability of **Rh-T** in detecting cellular Fe^{2+} pools.

Cell Imaging Studies

The ability of **Rh-T** to detect Fe^{2+} in primary human fibroblast cells (ws1) was investigated by using a confocal microscopy. Live ws1 cells incubated with 1 μM **Rh-T** showed weak fluorescence (Figure 4b). For Fe^{2+} repleting conditions, live ws1 cells were incubated with 100 μM of ferrous ammonium sulfate ($Fe(NH_4)_2(SO_4)_2$) at 37° C for overnight followed by washing with EMEM medium to remove excess Fe^{2+} and then 1 μM of **Rh-T** was added to the culture media and was incubated at 37° C for 30 min. The Fe^{2+}-treated ws1 cells showed significant increase in fluorescent signals (Figure 4c) w.r.t the ws1 cells without Fe^{2+} supplementation (Figure 4b), suggesting a positive response of **Rh-T** to increased labile Fe^{2+}levels in Fe^{2+} –treated cells. For Fe^{2+}-depleting conditions, 2, 2-bipyridyl (Bpy) which is known to be a selective Fe^{2+}–chelator was used to chelate Fe^{2+}[49-50]. Ws1 cells treated with 10 mM of Bpy showed decrease in fluorescence signal and it is weaker than that of the control cells (Figure 4e); suggesting **Rh-T** can detect basal level of labile Fe^{2+} in ws1 cells. The ws1 cells treated with 100 μM of Fe^{2+} overnight first followed by washing with EMEM medium and then treated with 10 mM of Bpy and subsequent addition of 1 μM of **Rh-T** showed marked decrease in fluorescent intensity (Figure 4d) compare to that of cells with Fe^{2+} supplement. This fluorescent intensity is almost the same as that of cells without Fe^{2+} or Bpy treatment. Contributions from endogenous protoporphyrin IX emitting [51] can be excluded as it does not absorb strongly in the excitation wavelength used in the study and the cells did not show any detectable fluorescent signal prior to the treatment of the **Rh-T** sensor. These data clearly demonstrate that **Rh-T** has the ability to detect endogenous level of labile Fe^{2+}as well as its dynamic changes in ws1 cells.

As the Fe^{2+}-activated **Rh-T** fluorescent signals display a non-diffusive pattern in cells, it offers the opportunity to find out the subcellular localization of Fe^{2+} in the cells. Co-localization experiments were performed with the help of MitoTracker Green FM and LysoTracker blue DND-22 in ws1 cells. Ws1 cells with Fe^{2+} supplementation showed strong fluorescent signals, which co-localize well with the signals from MitoTracker Green (Figure 5), suggesting a Fe^{2+} pool in mitochondria of ws1 cells. However, the Fe^{2+}-induced fluorescent images do not overlap with the images from LysoTracker blue (Figure S12). This could be initially interpreted as either low Fe^{2+} level or low **Rh-T** level in lysosomes. As **Rh-T** is a positive-charged rhodamine derivative and such species is known to preferentially targeting into mitochondria due to its negative membrane potential [52], it is more likely that **Rh-T** preferentially accumulates into mitochondria and detects the Fe^{2+} pools there. Thus this non-lyso co-localization data cannot exclude the possibilities of the existence of Fe^{2+} pools in lysosomes or elsewhere in cells. Nevertheless, these data confirms that the cellular Fe^{2+} pool in mitochondria and its dynamic changes are detectable by **Rh-T**.

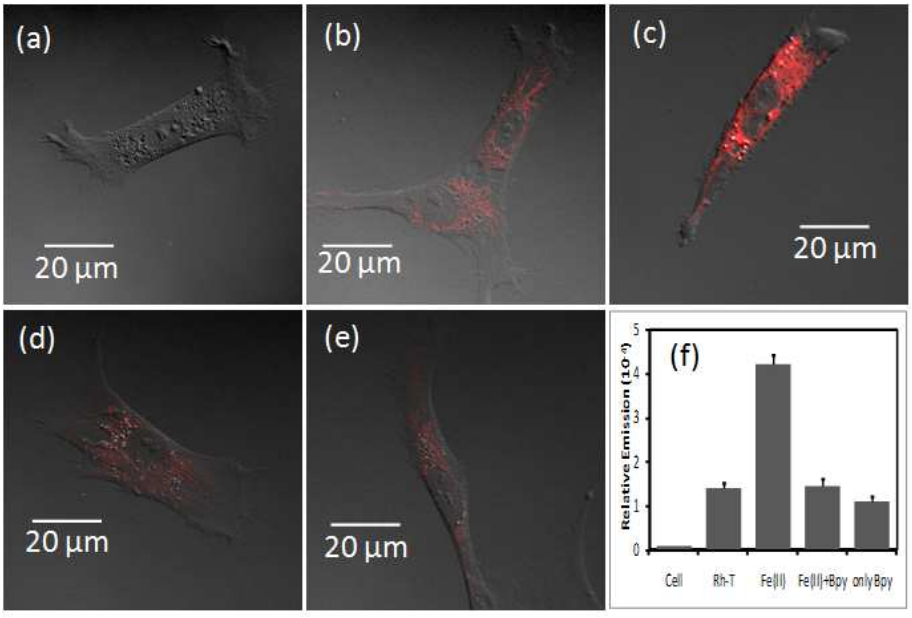

Fig. 4. Confocal microscopy images (with DIC) of live human ws1 fibroblast cells (contrast enhanced images were used for easier observation of the fluorescence pattern): (a) DIC image of cells with 20 μm scale bar and treated with; (b) 1 μM Rh-T at 37° C for 30 min; (c) 100 μM Fe^{2+} at 37° C for overnight and then treated with 1 μM Rh-T at 37° C for 30 min; (d)100 μM Fe^{2+} at 37° C for overnight and then 1 mM 2,2'-bipyridyl(Bpy) for 30 min at 37° C and then treated with 1 μM Rh-T at 37° C for 30 min; (e) 1 mM 2,2'-

bipyridyl(Bpy) for 30 min at 37° C and then treated with 1μM Rh-T at 37° C for 30 min; (f) Bar chart of the relative intensity of (a), (b), (c), (d) and (e).

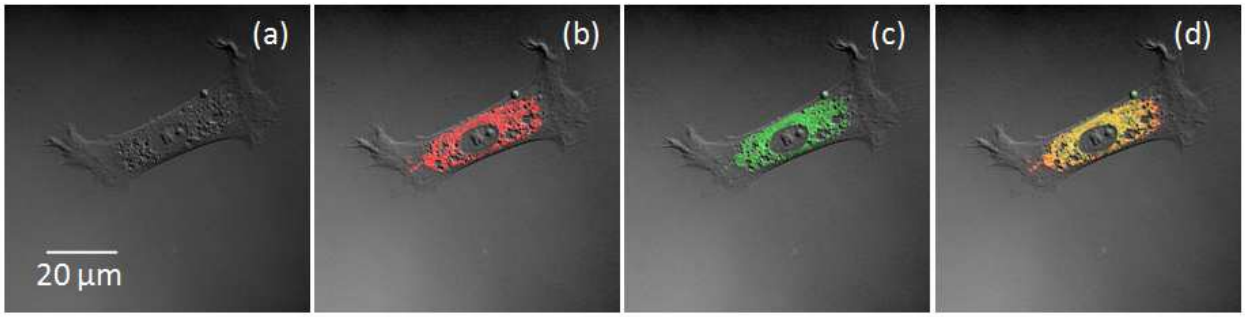

Fig.5. Representative confocal images of intracellular colocalization studies of 1 μM Rh-T incubated with ws1 cells co-labeled with MitoTracker Green (100 nM)). (a) DIC image of cells with 20 μm scale bar; (b) Rh-T-Fe^{2+}fluorescence collected at 547-703 nm (red); (c) MitoTracker fluorescence collected at 492-548 nm (green); (d) DIC image of (a) and fluorescence images of (b) and (c) were merged together. Colocalization regions are in yellowish.

Finally, we also tested the ability of **Rh-T** to detect Fe^{2+} in live human fibroblast ws1 cells via EPR spectroscopy. Ws1 cells were treated with 50 μM of **Rh-T** for 30 min at 37° C and then EPR experiments were performed. Compared to that of the untreated cells (Figure 6A), the EPR spectrum of the **Rh-T** treated cells showed a triplet spectrum which matches the EPR spectrum of **Rh-T** (Figure 6B). Next, ws1 cells were incubated with Fe^{2+} first followed by the addition of 50 μM of **Rh-T**. The EPR result shows that the triplet spectrum of **Rh-T** disappeared (Figure 6C), suggesting the specific redox reaction between the sensor and the over-loaded cellular Fe^{2+}, converting the Rh-T into diamagnetic species. The EPR spectrum of ws1 cells treated with 1 mM of Bpy for 30 min followed by the addition of 50 μM of **Rh-T**, showed the Rh-T triplet spectrum (Figure 6D) with increased intensity compared to that of the untreated cells (Figure 6B), implying the basal level Fe^{2+} was chelated by Bpy. The EPR results corroborate the conclusions from the confocal imaging studies that the sensor **Rh-T** is able to detect endogenous level of labile Fe^{2+}as well as its dynamic changes in ws1 cells.

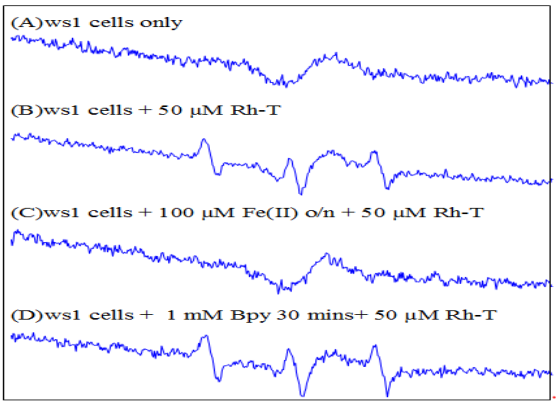

Fig.6. EPR spectra of live human ws1 fibroblast cells treated with Fe^{2+}, Bpy and Rh-T. (A) Cells in EMEM medium without Rh-T; (B) Cells in EMEM medium incubated with 50 μM Rh-T at 37° C for 30 min; (C) Cells in EMEM medium supplemented with 100 μM Fe^{2+} at 37° C for overnight and then treated with 50 μM Rh-T at 37° C for 30 min; (D) Cells in EMEM medium treated with 1 mM 2,2'-bipyridyl(Bpy) for 30 min at 37° C and then treated with 50 μM Rh-T at 37° C for 30 min.

Conclusions

In summary, we have developed highly selective reaction-based "turn-on" fluorescent sensors for Fe^{2+}, **Cou-T** and **Rh-T**, by tethering fluorophores with a nitroxide radical, which quenches the fluorescence. Fluorescent spectroscopy and EPR results support the reduction of the nitroxide radical by Fe^{2+} to produce a diamagnetic hydroxylamine species with fluorescence recovery (unmask). Confocal experiments with live human fibroblast ws1 cells demonstrated that **Rh-T** has the capability of detecting endogenous basal level Fe^{2+}, as well as the dynamic changes in cellular Fe^{2+}levels, i.e., externally supplemented Fe^{2+} or under depleting conditions. Co-localization experiments showed that **Rh-T** can detect labile Fe^{2+} pools in mitochondria of ws1 cells. Moreover, EPR spectra with cells corroborated the conclusions from the confocal imaging studies.

Notes and references

[a] S. Maiti, Y. Zhang, and M. Guo
Department of Chemistry and Biochemistry, University of Massachusetts Dartmouth, 285 Old Westport Road, Dartmouth, MA02747 (USA)
E-mail: mguo@umassd.edu
[b] S. Maiti and M. Guo
Biomedical Engineering & Biotechnology PhD Program, University of Massachusetts Dartmouth, 285 Old Westport Road, Dartmouth, MA, 02747 (USA)
[c] S. Maiti, Z. Aydin, Y. Zhang, and M. Guo
UMass Cranberry Health Research Center, University of Massachusetts Dartmouth, 285 Old Westport Road, Dartmouth, MA, 02747 (USA)
[d] Z. Aydin, M. Guo
Department of Chemistry, University of Massachusetts Amherst, 710 North Pleasant Street, Amherst, MA 01003 (USA)
E-mail: mguo@chem.umass.edu

†Electronic Supplementary Information (ESI) available: [details of any supplementary information available should be included here]. See DOI: 10.1039/b000000x./

We thank the National Science Foundation (CHE-1213838 and CHE-1229339) for financial support.

1 S. J. Lippard, J. M. Berg, *Principles of Bioinorganic Chemistry*, University Science Books, Mill Valley, CA,1994.

2 D. W. Domaille, E. L. Que , C. J. Chang, *Nat. Chem. Biol.*,2008, **4**, 168.

3 P. Aisen, M. Wessling-Resnick, E. A. Leibold*, Curr. Opin. Chem. Biol*., 1999, **3**, 200.

4 B. Halliwell, J. M. C. Gutteridge*, FEBS Lett*., 1992, **307**,108.

5 J. Xu, Z. Jia, M. D. Knutson, C. Leeuwenburgh, *Int. J. Mol.Sci*., 2012, **13**, 2368.

6 M. B. Youdim, D. Ben Shachar, S. Yehuda and P. Riederer, *Adv Neurol*.,1990, **53**,155.

7 B. Halliwell, J. M. C. Gutteridge, *Methods Enzymol* ,1990, **186**, 1.

8 S. P. Young, P. Aisen, The liver and iron. In The Liver : Biology and Pathobiology (Arias, I. M., Boyler, J. L. and Fausto, N., eds.), Raven Press, New York, 1990,597.

9 M. Roat-Malone, Bioinorganic chemistry; a short course, John Wiley and Sons, New Jersey, 2002,1.

10 S. Altamura, M. U. Muctkenthaler, *J. Alzheimer Dis*., 2009,**16**, 879.

11 R. Crichton, Inorganic biochemistry of iron metabolism; from molecular mechanisms to clinical consequences, John Wiley & Sons, Ltd Baffins Lane, Chichester, 2001.

12 Y. Kohgo, K. Ikuta, T. Ohtake, Y. Torimoto, J. Kato, *Int. J.Hematol*., 2008, **88**, 7.

13 W. Breuer, M. Shvartsman, Z. I. Cabantchik, *Int. J. Biochem. Cell Biol*., 2008, **40**, 350.

14 G. J. Anderson, C. D. Vulpe, *Cell. Mol. Life Sci*., 2009, **66**, 3241.

15 R. R. Crichton, S. Wilmet, R. Legssyer, R. J. Ward, *J. Inorg.Biochem*., 2002, **91**, 9.

16 E. Tomat, S. J. Lippard*, Curr. Opin. Chem. Biol*., 2010, **14**,225.

17 L. Yang, R. McRae, M. M. Henary, R. Patel, B. Lai, S. Vogt, C. J. Fahrni*,Proc.Natl.Acad. Sci.U. S.A*., 2005, **102**, 11179.

18 E. L. Que, D. W. Domaille, C.J. Chang**,** *Chem Rev*., 2008, **108**, 1517.

19 B.P. Esposito, S. Epsztejn, W. Breuer, Z.I. Cabantchik, *Anal. Biochem*., 2002, **304**, 1.

20 S. Fakih, M. Podinovskaia, X. Kong, U. E Schaible, H. L. Collins, R. C. Hider, *J. Pharmaceut. Sci.* , 2009, **98**, 2212.

21 S. Epsztejn, O. Kaklon, H. Glickscein, W. Breuer, Z. Cabantchik, *Anal. Bio. Chem*., 1997, **248**, 31.

22 F. Petrat, U. Rauen, H. de Groot, Hepatology, 1999**,29**, 1171.

23 B. P. Esposito, W. Breuer, P. Sirankapracha, P. Pootrakul, C. Hershko, Z. I. Cabantchik, *Blood*, 2003, **102**, 2670.

24 H. Glickstein, R. B. El, M. Shvartsman, Z. I. Cabantchik, *Blood*, 2005, **106**, 3242.

25 M. Wrona, K. Patel, P. Wardman, *Free Radical Biol. Med*., 2005, **38**, 262.

26 P. Li, L. Fang, H. Zhou, W. Zhang, X. Wang, N. Li, H. Zhong, B. Tang, *Chem.–Eur. J*., 2011, **17**, 10520.

27 L. Praveen, M. L. P. Reddy, R. L. Varma, *Tetrahedron Lett*., 2010, **51**, 6626.

28 T. Hirayama,K. Okudaand, H. Nagasawa, *Chem. Sci*., 2013, **4**, 1250.

29 H. Y. Au-Yeung, J. Chan,T. Chantarojsiri, C. J. Chang.*J. Am. Chem. Soc*. 2013, **135**, 15165.

30 D. R. Richardson, D. J. R. Lane, E. M. Becker, M. L.-H. Huang., M. Whitnall,Y. S. Rahmanto, A. D. Sheftel, P. Ponka, *PNAS*, 2010, **107**, 10775.

31 Y. Wei, Y. Zhang, Z.Liu, M. Guo, *Chem. Commun*., 2010, **46**(25), 4417.

32 Z. Aydin, Y. Wei, M. Guo, *Inorg. Chem. Commun.*, 2012, **20**, 93.

33 Y. Wei, Z. Aydin, Y.Zhang, Z. Liu and M. Guo, *ChemBioChem*, 2012, **13**(11), 1569

34 Y. Jiao, Y. Zhang, Y. Wei, Z. Liu, W. An, M. Guo, *ChemBioChem*, 2012, **13**(16), 2335.

35 Z. Aydin, Y. Wei, M. Guo*, Inorg.Chem.Commun*., 2014, **50**, 84.

36 A.Hassner,V. Alexani, *Tetrahedron Lett.,* 1978, **46**, 4475.

37 J.P. Blinco, K.E. Fairfull-Smith, B.J. Morrow, S.E. Bottle, *Aust.J.Chem*.,2011,**64**,373.

38 X. F. Yang, X. Q. Guo, *Analyst,* 2001, **126**, 564.

39 Y. Katayama, N. Soh, K. Koide, M. Maeda, *Chemm lett*., 2000, **29**, 1152.

40 J. L. Chen, C. Q. Zhu, *Microchim Acta*, 2007, **156**, 307.

41 Y.Kato, Y. Shimizu, L. Yuing, K. Unoura, H. Utsumi, T. Ogata, *Electrochim Acta*, 1995, **40**, 2799.

42 Y.Kashiwaqi, T. Nishimura, J. I. Anzai, *Electrochim Acta*, 2002, **47**, 1317.

43 H. Y. Ahn, K. E. Fairfull-Smith, B. J. Morrow, V. Lussini, B. Kim, M. V. Bondar,S. E. Bottle, K. D. Belfield, *J. Am. Chem. Soc*. 2012, **134**, 4721 .

44 P. G. Nogales, A. Almeida, J. P. Bolanos, *J. Biol. Chem*., 2002, **278**, 864.

45 A. Yamamoto, H. Tatsumi, M. Maruyama, T. Uchiyama, N. Okada, T. Fujita, *J. Pharmacol. Exp. Ther*., 2000, **296**, 84.

46 M. Guo, C. Perez, Y. Wei, E. Rapoza, G. Su, F. Bou-Abdallah and N. D. Chasteen, *Dalton Trans.*, 2007, (43), 4951.

47 L. Cao, Q. Wu, Q. Li, S. Shao, Y. Guo, *New J. Chem*., 2013, **37**, 2991.

48 H. Yang, T Yang, J. A. Baur1, E. Perez, T. Matsui, J. J. Carmona1, D. W. Lamming, N. C. Souza-Pinto, V. A. Bohr, A. Rosenzweig, R. Cabo, A. A. Sauve, D.A. Sinclair, *Cell*, 2007, **130**(6), 1095.

49 W.Breuer, S.Epsztejn, Z.I. Cabantchik, *J. Biol. Chem*., 1995, **270**, 24209.

50 A.M. Romeo, L. Christen, E.G. Niles, D.J.Kosman*, J. Biol. Chem*., 2001, **276**, 24301.

51 A.C. Croce, G. Santamaria, U. De Simone, F. Lucchini, I. Freitas, G. Bottiroli, *Photochem Photobiol Sci.* 2011,**10**, 1189.

52 Y. Zhou, S. Liu, *Theranostics.* 2012; **2**(10), 988.

DT-ART-12-2014-003792

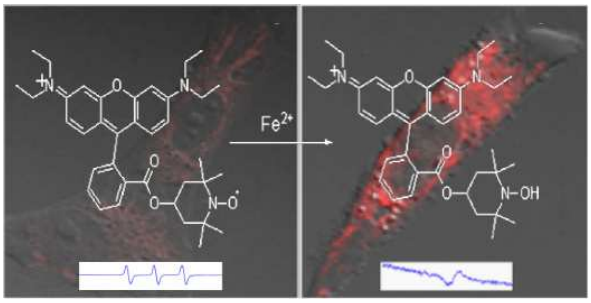

Highly selective reaction-based “turn-on” fluorescent sensor is capable of detecting Fe^{2+} in mitochondria with distinct EPR responses.